Monthly Notices
of the
ROYAL ASTRONOMICAL SOCIETY

Mon. Not. R. Astron. Soc. **406,** 2605–2615 (2010) doi:10.1111/j.1365-2966.2010.16854.x

First star formation with dark matter annihilation

E. Ripamonti,[1,2]★ F. Iocco,[3] A. Ferrara,[4] R. Schneider,[5] A. Bressan[6,7,8] and P. Marigo[9]

[1]*Università degli Studi di Milano-Bicocca, Dip. di Fisica 'G. Occhialini', Piazza della Scienza 3, I-20126 Milano, Italy*
[2]*Università degli Studi dell'Insubria, Dip. di Scienze Chimiche, Fisiche e Naturali, Via Valleggio 12, Como, Italy*
[3]*Institut d'Astrophysique de Paris, UMR 7095-CNRS Paris, Université Pierre et Marie Curie, 98bis Bd Arago, F-75014 Paris, France*
[4]*Scuola Normale Superiore, Piazza dei Cavalieri 7, Pisa, Italy*
[5]*INAF/Osservatorio Astrofisico di Arcetri, Largo Enrico Fermi 5, Firenze, Italy*
[6]*SISSA, Via Beirut 4, Trieste, Italy*
[7]*INAF/Osservatorio Astronomico di Padova, Vicolo dell'Osservatorio 5, Padova, Italy*
[8]*INAOE, Luis Enrique Erro 1, 72840, Tonantzintla, Puebla, Mexico*
[9]*Università degli Studi di Padova, Dip. di Astronomia, Vicolo dell'Osservatorio 2, I-35122 Padova, Italy*

Accepted 2010 April 15. Received 2010 April 15; in original form 2010 March 2

ABSTRACT

We include an energy term based on dark matter (DM) self-annihilation during the cooling and subsequent collapse of the metal-free gas, in haloes hosting the formation of the first stars in the Universe. We find that the feedback induced on the chemistry of the cloud *does* modify the properties of the gas throughout the collapse. However, the modifications are not dramatic, and the typical Jeans mass within the halo is conserved throughout the collapse, for all the DM parameters we have considered. This result implies that the presence of DM annihilations does not substantially modify the initial mass function of the first stars, with respect to the standard case in which such additional energy term is not taken into account. We find also that when the rate of energy produced by the DM annihilations and absorbed by the gas equals the chemical cooling (at densities yet far from the actual formation of a protostellar core) the structure does *not* halt its collapse, although that proceeds more slowly by a factor smaller than few per cent of the total collapse time.

Key words: stars: formation – stars: Population III – dark ages, reionization, first stars – dark matter.

1 INTRODUCTION

In the currently favoured Lambda cold dark matter (ΛCDM) cosmological model, the bulk of the matter component is believed to be made of (so far) electromagnetically undetected particles, commonly dubbed dark matter (DM). Although the evidence for the existence of DM is compelling on different scales, yet its nature is unknown, and many particle models beyond the standard one have been proposed in the literature as DM candidates. We address the reader to a recent review of observational evidence and particle candidates for DM (e.g. Bertone, Hooper & Silk 2005), and will concentrate in this paper on a particular class of candidates, i.e. weakly interacting massive particles (WIMPs). Many WIMP DM models are stable (under the conservation of the suitable symmetry, for each model) and hence do never decay into standard model particles. However, in many of these very same models the WIMPs are Majorana particles, thus carrying the remarkable property of being self-annihilating; the value of the self-annihilation cross-section, arising naturally in many WIMP models, reproduces the DM relic abundance required by the ΛCDM cosmology, if the mass scale of WIMPs is within the GeV/TeV scale and they are to be thermally produced in the early Universe. We adopt this as a benchmark scenario for our paper, and will often refer to it as a 'Vanilla WIMP'.

The actual DM distribution in the local Universe is such that even in the densest regions (e.g. galactic nuclei and black hole surroundings) from which the annihilation signal could be in principle detected, the energy released by WIMP DM annihilations (hereafter DMAs) is only a negligible fraction of the one associated with standard gas processes. This implies that, locally, DM affects the host system almost uniquely through its gravitational effects, perhaps with the only possible exception of peculiar locations, such as the central parsec of the Milky Way (Fairbairn, Scott & Edsjo 2008; Scott, Edsjo & Fairbairn 2009; Casanellas & Lopes 2009). The effects of annihilating (or decaying, a scenario we do not consider here) DM upon the evolution of the intergalactic medium (IGM) at high redshift have been thoroughly studied (e.g. Chen & Kamionkowski 2004; Mapelli & Ferrara 2005; Padmanabhan & Finkbeiner 2005; Furlanetto, Oh & Pierpaoli 2006; Mapelli, Ferrara & Pierpaoli 2006; Zhang et al. 2006; Ripamonti, Mapelli & Ferrara 2007a; Shchekinov & Vasiliev 2007; Valdés et al. 2007), and are now believed to be small, except perhaps in the case of an extremely high clumping factor (Chuzhoy 2008; Myers & Nusser 2008; Natarajan & Schwarz 2008; Lattanzi & Silk

★E-mail: ripamonti.e@gmail.com

2009), if one takes into consideration a standard, Vanilla WIMP scenario.

The effects of DMAs upon primordial star formation might be more significant. As the IGM could be heated by the energy deposition from DMAs, its temperature might in principle exceed the virial temperature of the smallest haloes with the result of quenching gas accretion on to them. This effect has been shown to be unimportant by Ripamonti, Mapelli & Ferrara (2007b, hereafter RMF07). However, DMAs are expected to become more important as the collapse proceeds to protostellar scales (Ascasibar 2007). Spolyar, Freese & Gondolo (2008, hereafter SFG08) found that during the protostellar collapse of the first (Population III) stars, the energy released by DMAs and absorbed by the gas could compensate (or even overcome) the radiative cooling of the gas. The increasing importance of such process arises from the combined enhancement during the collapse of DM density (due to gravitational dragging) and gas optical depth, implying a higher annihilation luminosity and absorption by the gas. The final phases of the collapse, after the formation of a hydrostatic core for gas central densities $n_c \equiv \rho_c/m_p > 10^{18}\,\mathrm{cm}^{-3}$ (where ρ_c is the central baryonic density, and m_p is the proton mass), have been investigated by Iocco et al. (2008, hereafter I08), Freese et al. (2008b, 2009) and Spolyar et al. (2009). Initially, the DM pile-up is purely driven by gravitational interactions, but as the protostar approaches the zero-age main sequence, DM accretion becomes dominated by the capture of WIMPs located in the star host halo after they scatter stellar baryons. As a consequence of the peculiar formation process of Population III, following the smooth collapse of the gas cloud at the very centre of the DM haloes hosting them, Iocco (2008) and Freese, Spolyar & Aguirre (2008a) suggested that DM capture is relevant for primordial stars; however, it can be safely neglected once local star formation is concerned, as the latter takes place anywhere in galactic discs, and it does not follow from a single, centred gas collapse episode. Further studies (I08; Taoso et al. 2008; Yoon, Iocco & Akiyama 2008) have concluded that WIMP DM capture's most remarkable effect is the possible increase of the stellar lifetime.

Quite surprisingly, the early phases of the collapse have received so far less attention with respect to the more advanced ones, i.e. after hydrostatic core formation. For example, it is still unclear if the energy injection following annihilations results in a net heating or cooling of the gas. In fact, high-energy photons and electrons heat the gas through ionizations; however, this heat input could be overwhelmed by the increased production of cooling species (as for example molecular hydrogen) stimulated by the larger abundances of free electrons, thus resulting in a net gas cooling. This, among others, is one of the aspects of the collapse of first stars in presence of WIMP annihilation that we would like to address here. We plan to do so by a set of sophisticated numerical simulations including all the relevant chemical reactions and cooling processes. A first attempt to model the effects of DMA energy input was presented in Ripamonti et al. (2009); this paper represents a substantial extension and improvement of that study.

Throughout the paper we assume the following set of cosmological parameters: $\Omega_\Lambda = 0.76$, $\Omega_m = 0.24$, $\Omega_b = 0.042$, $\Omega_{DM} = \Omega_m - \Omega_b \equiv \Omega_{WIMP} = 0.198$ and $h = 0.73$.

2 METHOD AND CODE

We base our investigation on a 1D spherically symmetric code described by Ripamonti et al. (2002, hereafter R02). The original code, which includes the treatment of gravitation, hydrodynamics and especially the chemistry and cooling of primordial gas, was originally conceived for the study of the last phases of the collapse of a primordial protostar (see also Omukai & Nishi 1998); later, it was extended in several ways (see Ripamonti 2007; Ripamonti et al. 2007a; RMF07).

Our simulations are based on those described in RMF07; here we list their most important properties, especially when they differ from RMF07.

(i) A single typical halo with mass $10^6\,\mathrm{M}_\odot$ virializing at $z = 20$ (virial radius $R_{vir} \simeq 5 \times 10^{20}$ cm) is considered; the baryon fraction inside such halo is assumed to be equal to the cosmological value ($\Omega_b/\Omega_{DM} \simeq 0.175$).

(ii) The simulations are started at $z = 1000$ and involve a comoving volume 1000 times larger than that of simulated halo; initial baryonic density and temperature are constant in all the simulation shells, and equal to the cosmological values.

(iii) Before virialization, the gravitational effects of DM are treated as in the NFW case of RMF07: a pre-determined (but time-dependent until virialization) DM potential is added to the gas self-gravity. Such potential mimics the evolution of a halo in the top-hat approximation: as the DM potential becomes steeper, the (initially uniform) gas falls towards the centre of the halo, similarly to what is predicted by theory and consistent with the results of simulations (see e.g. fig. 2 of Abel, Bryan & Norman 2002).

(iv) After virialization, the evolution of the previously described artificial DM potential is stopped: its state at virialization is set to a NFW profile (Navarro, Frenk & White 1996) with $c = 10$ and $R_{200} = R_{vir}$; this is reasonably close to the results shown in fig. 2 of Abel et al. (2002). The evolution of the DM profile is also followed in response to the baryon contraction (see later) in order to compute the DMA rate.[1]

(v) RMF07 investigated *whether* stellar formation might occur in a halo, whereas here we investigate *how* it starts; for this reason, simulations are stopped only when their computational costs become very large (usually at number densities $n_c \approx 10^{14}\,\mathrm{cm}^{-3}$).

(vi) The DM energy input is computed only after halo virialization, and only in regions with high baryon density ($\rho \geq 4 \times 10^{-22}\,\mathrm{g\,cm}^{-3}$, i.e. $n \equiv \rho/m_p \gtrsim 250\,\mathrm{cm}^{-3}$), rather than at all times and everywhere: this is because RMF07 already showed that before virialization and at low baryon densities the effects of DMAs are small.

(vii) For the purpose of evaluating the DMA rate (see below), the DM density $\rho_{DM}(r)$ is evaluated by assuming the conservation of the so-called 'adiabatic' invariant (see Blumenthal et al. 1986). We implement the algorithm described by Gnedin et al. (2004), following the details in I08, and using the NFW and gas profiles described above as initial conditions.[2]

(viii) The specific luminosity due to DMAs is

$$l_{DM} = c^2 \langle \sigma v \rangle \, \rho_{DM}^2/(m_{DM}), \quad (1)$$

where $\langle \sigma v \rangle$ is the thermally averaged annihilation rate, and m_{DM} is the WIMP mass; in the following we adopt $\langle \sigma v \rangle = 3 \times 10^{-26}\,\mathrm{cm}^3\,\mathrm{s}^{-1}$, whereas we consider m_{DM} as a free parameter in

[1] We do not account for the gravitational effects of the adiabatically contracted DM profile because adiabatic contraction (AC) is effective only when the baryonic potential largely dominates over the DM.

[2] It is to be noted that the DM profile in (gravitationally) baryon-dominated regions is eventually dictated by the amount of gas accumulated after the contraction, see e.g. fig 1 in SFG08. Our conclusions, especially regarding the final phases of the collapse, are hence almost insensitive to the initial DM profile.

the range $1.78 \times 10^{-24} \leq m_{\rm DM} \leq 1.78 \times 10^{-21}$ g (i.e. 1 GeV $\leq m_{\rm DM} c^2 \leq 1$ TeV).

(ix) The energy ϵ that each baryon actually absorbs from DMAs (per unit time) is calculated through a detailed radiative transfer calculation, formally identical to the one performed for grey continuum radiation. Such calculation is based on a constant gas opacity $\kappa = 0.01\,{\rm cm^2\,g^{-1}}$ (roughly similar to the values used by SFG08). Moreover, since it is believed that the energy from annihilations splits roughly equally into electrons, photons and neutrinos, we assume that only 2/3 of $l_{\rm DM}$ (i.e. the fraction not going into neutrinos) can be absorbed.

(x) Similar to RMF07, ϵ can go into ionization, heating and excitation of atoms and molecules; we employ the results of Valdès & Ferrara (2008) (see also Shull & van Steenberg 1985; Furlanetto & Johnson Stoever 2010) to estimate how to split the energy input into these three. Also note that the 'ionization' component is split into ionization of H, D, He and He^+, and dissociation of H_2, HD and H_2^+. In our 'standard' treatment each species receives a fraction of the ionization energy which is proportional to its total baryonic content (in number, see RMF07 for details).

(xi) R02 switched to equilibrium chemistry (e.g. allowing the use of Saha equations instead of the detailed balance ones) for shells with number densities $n \geq 10^{13.5}\,{\rm cm^{-3}}$. Here we drop this simplification since (i) DMA effects change the chemical evolution of the gas, and usually delay the approach to equilibrium[3] and (ii) we never venture to densities $n > 10^{15}\,{\rm cm^{-3}}$.

Given the standing ignorance on the precise detail of feedback effects on the ionization and dissociation of atoms and molecules (especially H_2), in addition to the standard, fiducial set of runs we performed runs with either enhanced or reduced feedback, in order to bracket the possible impact of such process. In the same way, since the opacity κ we employ represents only a very rough estimate, we performed runs with either higher or lower values of κ.

3 RESULTS

We test the effects of DMAs varying different sets of parameters: (i) the normalization of the DMA rate, which is regulated by the ratio $\langle\sigma v\rangle/m_{\rm DM}$; (ii) the feedback strength on chemistry and (iii) the 'grey' gas opacity κ. We anticipate that the strength of feedback on chemistry has little impact on the overall results, and that the effects of a variation in κ are somewhat similar to a variation of the same amount in $\langle\sigma v\rangle/m_{\rm DM}$. We will discuss the dependence on these two latter parameters in Section 3.3.

Here we start by introducing in more details the physics of first star formation in presence of DMAs for our fiducial models ('M' labelled runs, see Table 1 for details). It is worth anticipating that the effects of DM become more relevant (and they become efficient earlier during the collapse) for higher self-annihilation cross-sections/lower DM masses (see equation 1). In what follows, we always adopt $\langle\sigma v\rangle = 3 \times 10^{-26}\,{\rm cm^3\,s^{-1}}$, and vary the particle mass $m_{\rm DM}$. Given the degeneracy in the DMA energy-injection term, the results can be interpreted at fixed mass and correspondingly varying the self-annihilation rate.

[3]Even in the few cases where it is possible to switch to the equilibrium chemistry (e.g. the 'control' run where we do not consider DMAs) we prefer to keep integrating the non-equilibrium equations in order to get results which are completely consistent with those from the other runs.

Table 1. Properties of the runs.

Name	$m_{\rm DM}c^2$ (GeV)	H_2 fbk	Notes
M1000	1000	std.	Minimal
M100	100	std.	Fiducial
M10	10	std.	Submaximal
M1	1	std.	Maximal
N1000	1000	off	
N100	100	off	
N10	10	off	
N1	1	off	
E1000	1000	enh.	
E100	100	enh.	
E10	10	enh.	
E1	1	enh.	
L100	100	std.	$\kappa = 0.001\,{\rm cm^2\,g^{-1}}$
L10	10	std.	$\kappa = 0.001\,{\rm cm^2\,g^{-1}}$
L1	1	std.	$\kappa = 0.001\,{\rm cm^2\,g^{-1}}$
H1000	1000	std.	$\kappa = 0.1\,{\rm cm^2\,g^{-1}}$
H100	100	std.	$\kappa = 0.1\,{\rm cm^2\,g^{-1}}$
H10	10	std.	$\kappa = 0.1\,{\rm cm^2\,g^{-1}}$
NODM	–	–	Control

Note. The first letter of the name of a run indicates the set to which it belongs; 'M' refers to the main set, 'N' to the set without DMA feedback upon H_2 formation, 'E' to the set with enhanced DMA feedback upon H_2 formation, 'L' to the set with low opacity and 'H' to the set with high opacity. The grey opacity is set to $\kappa = 0.01\,{\rm cm^2\,g^{-1}}$ for all of the runs presented in this table, except for runs in the 'L' and 'H' sets. The NODM run assumes no energy input from DMAs.

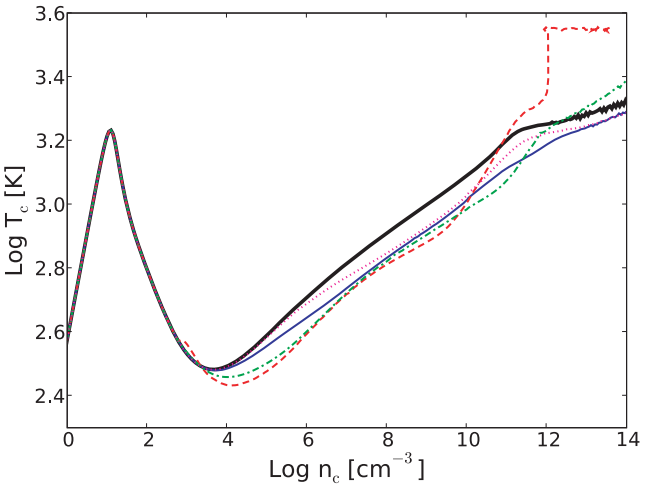

Figure 1. Evolution of the temperature $T_{\rm c}$ of the central shell of our simulation (whose mass is $\simeq 2 \times 10^{-4}\,{\rm M_\odot}$) as a function of its baryon number density $n_{\rm c}$, starting slightly before virialization. The thick solid line shows the evolution in the control run with no DM energy input (NODM). The thin solid line corresponds to the fiducial model (run M100); the dashed line to the maximal model (M1); the dot–dashed line to the submaximal model (M10) and the thin dotted line to the minimal model (M1000).

Fig. 1 shows the evolution of the temperature $T_{\rm c}$ of the innermost shell as a function of the density of the same central shell of the simulated objects ($n_{\rm c}$), for the five most representative models, M100, M10, M1, M1000 and NODM (see Table 1).

As expected, DMA effects, which can be quantified by the deviations from the thick solid line, are most prominent in runs with low-mass particles $m_{\rm DM}c^2 = 1$ GeV (M1 run, corresponding to the maximal DMA energy-injection rate), and become very limited in

the case of DM particles with high mass $m_{\rm DM}c^2 = 1$ TeV (M1000 run, minimal DMA energy-injection rate); we will comment extensively on such dependence later in this section. In the following we will refer to the 'fiducial' run (M100; where the choice of parameters is quite standard), to the 'minimal' run (M1000; where the high value of $m_{\rm DM}$ reduces the energy injection from DMAs, providing a check on the level where its effects become negligible), to the 'maximal' run (M1; where the parameters are chosen in a way which maximizes the energy injection from DMAs and their effects upon the gas evolution), and to the 'submaximal' run, M10. The maximal model, M1, is likely to represent a sort of upper limit on the effects of DMAs on the formation of primordial stars. In fact, the DM parameters corresponding to this run ($\langle\sigma v\rangle = 3 \times 10^{-26}$ cm^3 s^{-1}, $m_{\rm DM}c^2 = 1$ GeV) are currently severely disfavoured by multimessenger constraints on DM, in particular by (astrophysical) parameter-independent ones (e.g. Cirelli, Iocco & Panci 2009; Galli et al. 2009).

3.1 The indirect feedback phase

Fig. 2 compares the total energy input from DMAs into the gas (which needs to be splitted into ionizations, heating and excitations) to the cooling rate due to H_2. This comparison largely oversimplifies the thermal balance (see next subsection); however, it

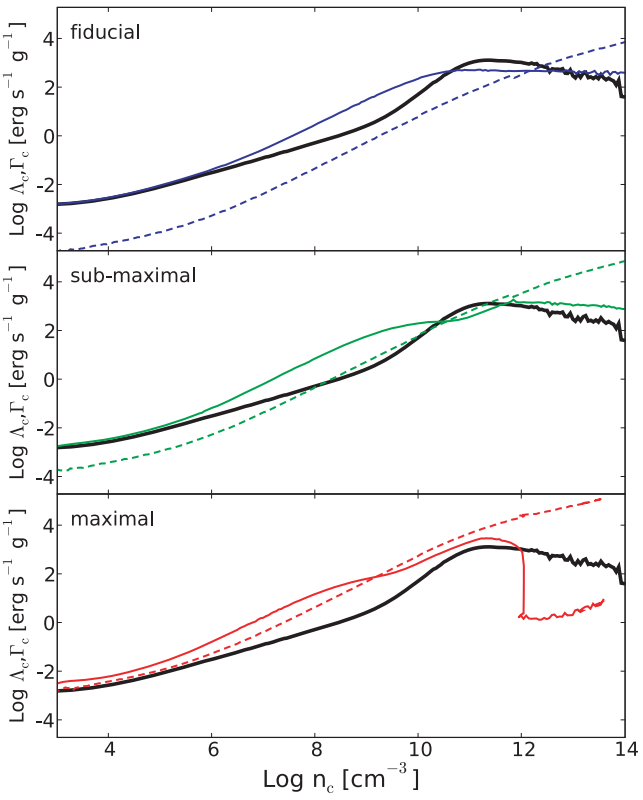

Figure 2. Evolution of the H_2 cooling rate and the rate of DMA energy input in the central shell of our simulations, as a function of its number density. In each panel the H_2 cooling rate (thin solid line) and the DMA energy input (dashed line) for one of our runs (from top to bottom: fiducial, submaximal and maximal runs) are compared to the H_2 cooling rate in the control NODM run (thick solid line). We note that the actual heating rate from DMAs is about 1/3 of what is shown here since the total DMA energy input also includes energy actually going into excitations and ionizations (see text for details).

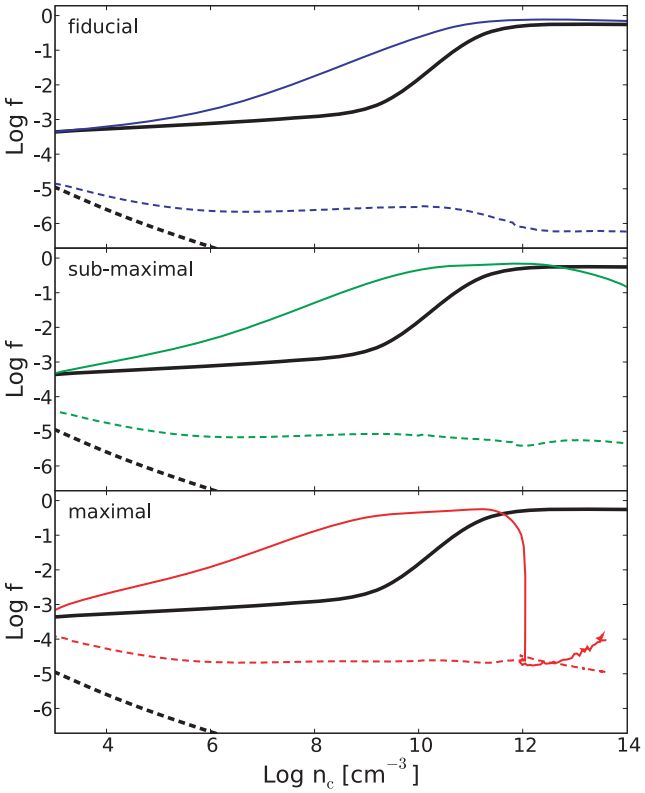

Figure 3. Evolution of the H_2 and e^- fractions in the central shell of our simulation as a function of its baryon number density. In each panel the H_2 fraction (thin solid line) and e^- fraction (thin dashed line) from one of our runs (from top to bottom: fiducial, submaximal and maximal runs) are compared to the same quantities from the control NODM run (thick solid line for H_2 and thick dashed line for e^-).

makes clear that, even in the maximal case, the heating from DMAs remains a relatively small fraction of the H_2 cooling until n_c becomes $\gtrsim 10^9$ cm^{-3}. At earlier stages (i.e. lower densities) the effects of DMAs are more subtle than what could be simply inferred by the direct heating, which would not be able to significantly change the temperature of the gas. In fact, it is quite remarkable that in the $10^3 \lesssim n_c \lesssim 10^{11}$ cm^{-3} range, the *additional* energy injection from DMAs results in a *decrease* of the central temperature (see also Fig. 1).

Such counterintuitive temperature decrease is due to indirect effects of DMAs, and in particular to their feedback on the chemistry; this remarkable property clearly emerges upon inspection of the curves in Fig. 2 showing that H_2 cooling (thin solid line) is stronger when DMAs are included (at least for $n_c \lesssim 10^{10}$ cm^{-3}).

In fact, as it can be inferred from Fig. 3, DMA *ionization* effects keep the gas more ionized than in the NODM case (i.e. e^- abundance 10^{-6} to 10^{-4}, rather than $\ll 10^{-6}$). In turn, this relatively high ionization level favours the formation of H_2 through the reaction chain

$$\mathrm{H} + \mathrm{e}^- \rightarrow \mathrm{H}^- + \gamma, \tag{2}$$

$$\mathrm{H}^- + \mathrm{H} \rightarrow \mathrm{H}_2 + \mathrm{e}^-, \tag{3}$$

which is the main formation route for H_2 in moderately dense, dust-free gas, and where the electrons act as catalysts (see e.g. Galli & Palla 1998; Glover & Jappsen 2007; Stasielak, Biermann & Kusenko 2007).

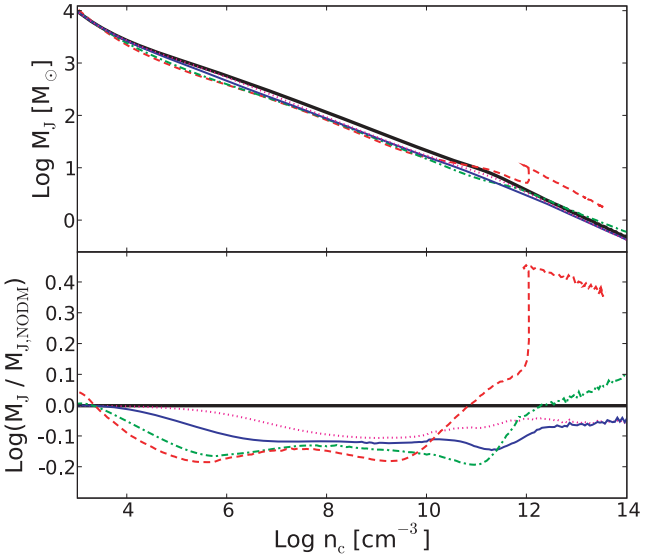

Figure 4. Evolution of the Jeans mass calculated using the density and temperature in the central shell of our simulation, as a function of its number density. Lines refer to the minimal (M1000; dotted), fiducial (M100; thin solid), submaximal (M10; dot–dashed) and maximal (M1; dashed) models, and to the control run (NODM; thick solid). The top panel shows the absolute value of M_J, whereas the bottom panel compares the various models by showing the ratio of M_J in a given model to $M_{J,NODM}$ in the NODM run.

As Ripamonti et al. (2009) remarked, the increase in the H_2 fraction can amount to two to three orders of magnitude, which apparently might imply same order-of-magnitude differences in the cooling rate, and large differences also in the gas temperature. However, while the increase in the cooling rate is quite large (though smaller than what is naively expected from the difference in H_2 abundance), the corresponding reduction of the gas temperature is much smaller, of the order of 30 per cent (see Fig. 1). This is due to the very strong temperature dependence of H_2 cooling, especially below ∼500 K (the temperature corresponding to the transition from the fundamental state to the lowest rotationally excited level): in fact, in this regime a moderate reduction in temperature results in a much larger decrease in the H_2 cooling rate, which in turn slows down the temperature decrease.

As a result, since the Jeans mass sensitivity to the temperature is quite mild,

$$M_J(n, T) \simeq 50\,M_\odot \left(\frac{T}{1\,K}\right)^{3/2} \left(\frac{n}{1\,cm^{-3}}\right)^{-1/2}, \quad (4)$$

DMAs might reduce the Jeans mass scale but only by a factor of $\lesssim$2 (see Fig. 4).

3.2 The direct feedback phase

Fig. 2 shows that when the density increases above $n_c \sim 10^{12}$ cm^{-3} ($\sim 10^9$ cm^{-3}) for the fiducial (maximal) run, the energy input from DMAs finally overcomes the H_2 cooling (see also Table 2 for details and a comparison with previous literature). This marks the beginning of what we call the direct feedback phase of the collapse since the DMAs' *direct* effects (especially the heating) finally start to dominate both H_2 cooling and the more subtle DMAs' indirect effects discussed above. We will refer to this condition (equality of DMA heating and H_2 cooling terms) as to the 'critical point'.

The study of this phase is particularly interesting because when the DMA heating starts to compensate the radiative cooling, the protostar becomes unable to shed away its gravitational energy; it had been previously proposed (see SFG08) that this could induce the stop of the collapse, and the formation of a new type of stable astrophysical object powered by DMAs.

Table 2. Density and temperatures where the total energy input from DMAs overcomes H_2 cooling.

$m_{DM}c^2$ (GeV)	n_{crit} (cm^{-3})	T_{crit} (K)
1[a]	1.5×10^9 (∼10^9)[b]	780 (∼800)[b]
10[a]	4.0×10^{10} (∼ 10^{11})[b]	1070 (∼1000)[b]
100[a]	1.3×10^{12} (∼10^{13})[b]	1580 (∼1300)[b]
1000[a]	8.0×10^{12} (∼ 10^{14})[b]	1740 (∼1400)[b]

[a]The quantities in this table are almost independent of the assumptions about the strength of H_2 feedback, so we do not distinguish among runs with the same m_{DM}.
[b]Numbers in brackets indicate the results which can be estimated from fig. 2 of SFG08, intersecting the Yoshida et al. (2006) curve with the curves for various DM masses; for the SFG08 1 GeV mass case we adopt the 100 per cent H_2 line.

The evolution of all the quantities beyond the critical point, shown in Figs 1 and 2, imply the existence of a dynamical evolution of the system also after the onset of the direct feedback phase – and hence no stalling of the object – even if there are important differences among the various runs.

In the fiducial run, the evolution of the central shell proceeds relatively undisturbed. For $n_c \leq 10^{14}$ g cm^{-3} the central temperature remains below the one of the control runs, even if the gap tends to close (see Fig. 1). Conversely, in the maximal run there is a substantial steepening of the evolution in the n_c–T_c plane, and the central temperature overcomes the value of the control run at $n_c \sim 10^{11}$ cm^{-3}. The temperature increase becomes particularly dramatic, with a sudden rise by a factor of ∼2 when the central density reaches $n_c \sim 10^{12}$ cm^{-3}.

In order to understand this phase, we need to describe the heating and cooling processes in detail. Fig. 5 shows the contributions from the main heating and cooling mechanisms during the contraction of the central shell, for our reference runs.

3.2.1 *Details of chemical cooling*

Fig. 5 shows the large importance of chemical heating/cooling, i.e. of the energy which is released/absorbed as a consequence of chemical reactions, and in particular (in this regime, at least) of the formation/dissociation of H_2 molecules[4]: in every run there is a phase where H_2 formation is the main heating mechanism. In the control run, chemical heating dominates over the adiabatic heating in the $10^{9.5} \lesssim n_c \lesssim 10^{12.5}$ cm^{-3} density range, which coincides with the regime where three-body reactions (see Palla, Salpeter & Stahler 1983) turn most of the hydrogen into molecular form. In the runs with DMAs such a phase is even more extended, as the DMA feedback on the chemistry anticipates the epoch of rapid H_2 formation: in the maximal run, chemical heating becomes dominant already at $n_c \gtrsim 10^{3.5}$ cm^{-3}.

[4]The formation of a H_2 molecule releases its binding energy (4.48 eV); at the densities we are considering here, most of this energy is eventually converted into thermal energy of the gas (see e.g. Hollenbach & McKee 1979); on the other hand, the dissociation of H_2 through collisional reactions absorbs the same amount of thermal energy from the gas.

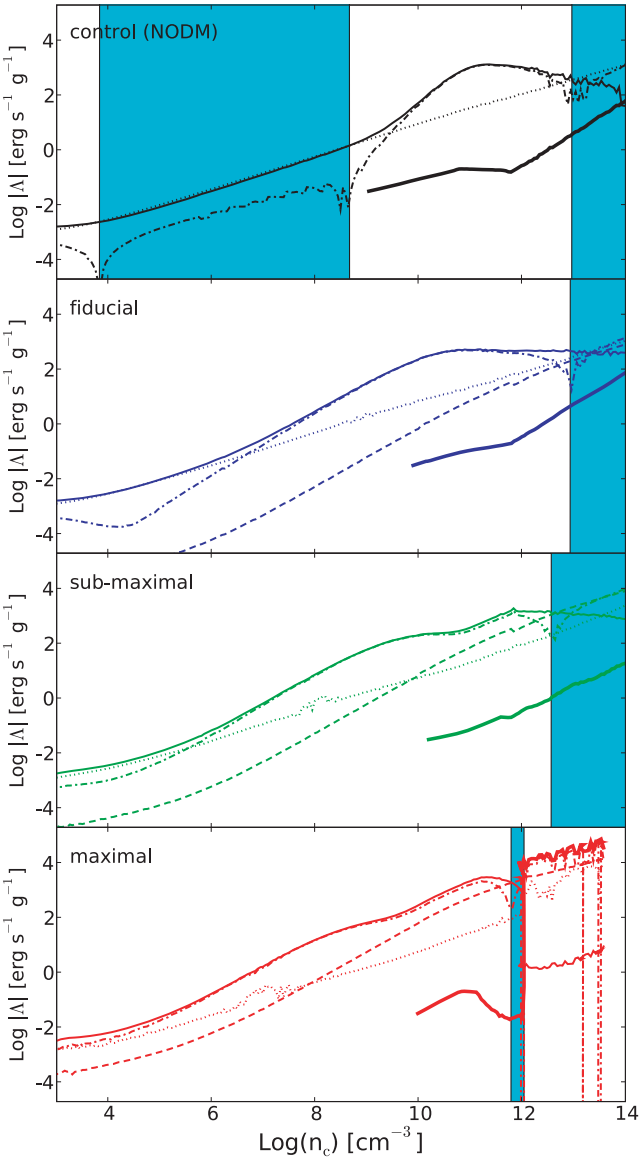

Figure 5. Evolution of the main heating and cooling mechanisms in the central shell of our simulations, as a function of its number density n_c. The panels refer to four different runs: from top to bottom, we show results for the control (without DMAs), fiducial, submaximal and maximal runs. Each panel shows H_2 line cooling (thin solid line), continuum cooling (thick solid line), DMA heating (dashed line), adiabatic heating (dotted line) and chemical heating or cooling (dot–dashed line). We note that (i) the continuum cooling line can be plotted only when $T_c \geq 1000\,\mathrm{K}$ (corresponding to $n_c \gtrsim 10^9$–$10^{10}\,\mathrm{cm}^{-3}$); however, it is negligible at lower temperatures; (ii) the DMA heating is different from the DMA energy input shown in Fig. 2 since it does not include the ionization and excitation components; (iii) the chemical term does not have a constant sign: shaded regions indicate the density ranges where it corresponds to a cooling term, whereas the ranges where it corresponds to a heating term are not shaded.

It is remarkable that the chemical term can contribute both to heating and cooling. It was already known (see e.g. Omukai & Nishi 1998; R02) that because of this property, it tends to act as a 'thermostat' which stabilizes the evolution of the collapse, even if it cannot always prevent sudden transitions.

The evolution of the maximal and submaximal models is particularly significant in this respect. In these models the H_2 fraction peaks (at a level $\gtrsim$0.8; see Fig. 3) when $n_c \simeq 10^{11}$–$10^{12}\,\mathrm{cm}^{-3}$: in such conditions three-body H_2 formation is slowed down by the relative scarcity of atomic H left, and must compete with the increasingly large number of dissociations due to the ionization component of the DMA energy input.[5]

When the molecular fraction starts to go down, the cooling rate must follow because it is dominated by H_2 and the number of molecules is being reduced; but so does the heating because its dominant component (chemical heating) is reduced by the energy lost in molecular dissociations. The fact that both the heating and the cooling mechanisms follow the same trend prevents a significant steepening of the temperature evolution and the consequent stop in the protostellar collapse. This is because the 'excess' energy which is not radiated away is mainly used to dissociate H_2.

However, this cannot last indefinitely, as the reservoir of H_2 is finite, and the DMA energy injection increases with increasing density. In the case of the maximal run, where the DMA energy injection is quite high, H_2 is rapidly exhausted. At $n_c \simeq 10^{12}\,\mathrm{cm}^{-3}$ there is essentially no H_2 left, which also implies almost no radiative cooling. Then, the temperature goes up very fast (see Fig. 1), developing a pressure gradient which is able to momentarily stop the collapse of the innermost shell (actually, there is even a very brief re-expansion episode – more details are discussed in Section 3.4); however, the increase in temperature also results in a very strong increase in the continuum radiation which is produced by collision-induced emission, H^-, and atomic H: continuum radiation increases by some six orders of magnitude (cf. Lenzuni, Chernoff & Salpeter 1991; Marigo & Aringer 2009) and replaces H_2 line radiation as the main cooling mechanism for the gas. The collapse is then able to resume, even if further investigations are needed in order to understand its details beyond $n_c \approx 10^{13}\,\mathrm{cm}^{-3}$. At present in fact, computational costs become almost unaffordable beyond $n_c \approx 10^{13}\,\mathrm{cm}^{-3}$ because of the strong sensitivity of cooling rate on temperature. In spite of these limitations we consider the conclusions based on these runs very robust as we have pushed the evolution to densities exceeding 10^4 times the 'critical' density at which the H_2 cooling becomes comparable to the DMA energy transferred to baryons.

Things are quite different in the case of the submaximal run: here a moderate H_2 dissociation rate can compensate both the heating and the ionization parts of the (relatively small) DMA energy input for a significant span. In fact, at $n_c = 10^{14}\,\mathrm{cm}^{-3}$ (i.e. at a density $\sim$100 times larger than the density at the onset of H_2 dissociation, and $\sim$1000 times larger than the density at the 'critical point') the H_2 fraction is still $\gtrsim$0.1: it is still possible that H_2 exhaustion (which we expect to happen at $n_c \sim 10^{15}\,\mathrm{cm}^{-3}$) is accompanied by a transition similar to the one we discussed for the maximal case; however, such transition is likely to involve a smaller adjustment in temperature (say, an increase by a factor of $\sim$1.5 rather than $\sim$2) because the required increase in the continuum cooling is much smaller (somewhat less than three orders of magnitude rather than six, as can be inferred from Fig. 5) than what was required in the maximal case.

[5]It is important to note that the DMA energy injection which goes into ionizations actually contributes to the chemical heating. For example, if the number density of H_2 molecules remains constant because the rate of formation (through three-body reactions) is compensated by the rate of dissociations induced by the DMAs, the chemical heating term will be positive. In fact, the energy released by H_2 formation ends up in the form of thermal energy, whereas the energy for the dissociations is *not* taken away from the gas thermal energy, as it is provided by DMAs.

The fiducial and minimal runs exhibit trends which are somewhat similar to the submaximal run: the peak in the H_2 abundance at $n_c \sim 10^{12}\,cm^{-3}$ is followed by an extremely slow decline, during which the adiabatic heating is often as important as the DMA heating: then, it is quite likely that the transition from H_2 line cooling to continuum cooling is as smooth as in the scenario without DMAs. In fact, it should be noted that at $n_c = 10^{14}\,cm^{-3}$ the continuum cooling amounts already to about 10 per cent of the total heating, and it is increasing faster than any heating mechanism (see Fig. 5).

3.3 Sensitivity to feedback and opacity

In order to check the effect of our assumptions about H_2 feedback (in particular, destruction of H_2 molecules by the energy injected by DMAs into the gas) we have run two extra sets of simulations: the first (label: E) in which H_2 feedback is enhanced, and the second (label: N) with DM-induced H_2 dissociations switched off. In the E models, we have assumed that *all* DMA energy input which goes into excitations is in the form of photons in the Lyman–Werner band ($11.2 \leq h\nu \leq 13.6\,eV$), and that each of these photons dissociates one H_2 molecule.[6] This clearly represents an upper limit on the feedback upon H_2, as in reality about half of the photons going into dissociations has energy below the lower limit of the Lyman–Werner band; furthermore, in low-density regions a significant fraction of Lyman–Werner photons can escape.

As it can easily be noted from the upper panel of Fig. 6 (showing the evolution of models M1, E1 and L1 in the n_c–T_c plane) switching off the H_2 feedback results in a sensible change of the temperature only in the final stages of collapse (because the absence of DMA-induced H_2 dissociations strongly reduces the heating); on the other hand, strengthening the feedback results in appreciable modification of the temperature of the cloud in earlier stages (because it reduces the H_2 abundance), but the difference reduces drastically in later phases (when the direct effects of DMAs dominate the ones on chemistry). We also note that in models with $m_{DM}c^2 \geq 10\,GeV$ the differences induced by the treatment of feedback are much smaller than in the models shown in Fig. 6 (with $m_{DM}c^2 = 1\,GeV$).

We have also studied the effects of varying the grey opacity κ, by running sets of simulations in which we have increased/decreased the fiducial value $\kappa = 0.01\,cm^2\,g^{-1}$ by one order of magnitude. At low and intermediate densities the effects on the evolution of the cloud are very similar to those of a decrease/increase of the particle mass m_{DM}; whereas models with the same m_{DM} tend to converge at high densities. In fact, an opacity variation affects sensibly the properties of the gas only when it is of 'optically thin' to the energy produced by DMAs: in later stages of the collapse (i.e. in regions of the halo where the gas is 'optically thick' to the DMA energy), the energy absorption does not depend on κ. This can be appreciated from the lower panel of Fig. 6, where it is clear that the modified opacity models (H, L labelled) overplot to the corresponding standard models (M labelled) at higher central densities.

We can definitely infer that 'astrophysical' (and 'numerical') parameter dependence is mostly degenerate with DM parameters,

[6]In practice, we assume a Lyman–Werner H_2 dissociation rate (per unit volume) equal to $n\epsilon f_{exc}/\bar{E}_{LW}$, where n is the baryon number density, ϵ is the energy input per baryon due to DMAs, f_{exc} is the fraction of this energy which goes into excitations (i.e. into photons with $10.2 \leq h\nu \leq 13.6\,eV$), and $\bar{E}_{LW} \simeq 12\,eV$ is the average energy of a Lyman–Werner photon. Such rate is added to the one produced by the fraction the DMA energy input which goes into ionizations.

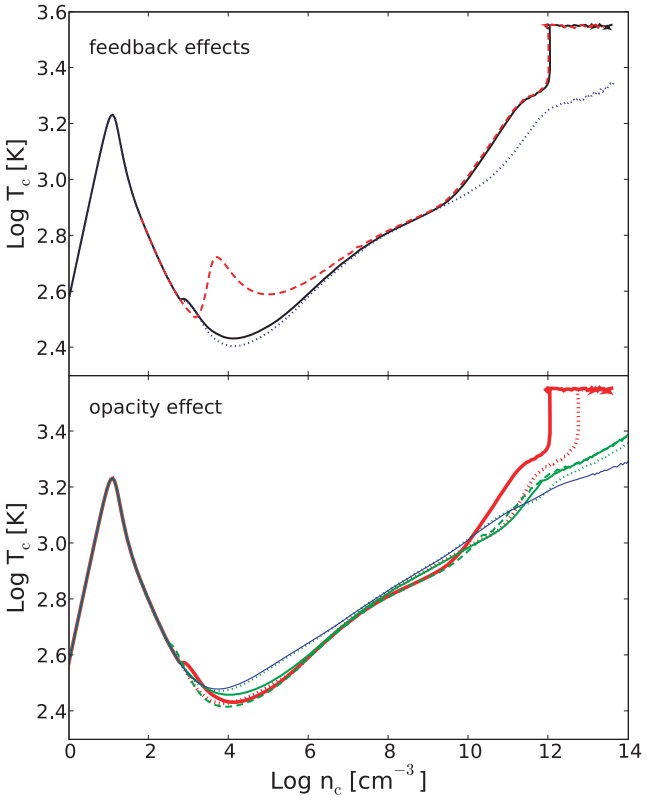

Figure 6. Effects of H_2 feedback schemes (upper panel) and opacity (lower panel): in the upper panel the solid represents the maximal run M1, the dashed line is the E1 run (case with enhanced H_2 feedback) and dotted line is the N1 run (no H_2 feedback). In the lower panel thick lines represent the M1 (solid) and L1 (dotted) runs, the intermediate lines represent the M10 (solid), L10 (dotted) and H10 (dashed); finally, the thin line is our fiducial M100 run. See text for details and Table 1 for run coding.

and in any case not drastically affecting the qualitative picture we have drawn so far.

3.4 The evolution of spatial profiles

3.4.1 The fiducial run

Fig. 7 shows the spatial profile of gas properties at four different stages (corresponding to central shell gas densities $n_c = 10^5, 10^8, 10^{11}$ and $10^{14}\,cm^{-3}$) in the M100 fiducial case and, for comparison, in the NODM control run. The top left-hand panel shows also the DM density in the case of M100 run at the same stages (DM density stays constant and equal to the initial profile in the NODM control run).

The first important remark to file is that the gas density profiles are virtually unchanged by the presence of DMAs: such profiles are indistinguishable until central gas densities of $n_c \sim 10^8\,cm^{-3}$ are reached, and even then the discrepancies are of minor entity (e.g. the slope outside the core becomes $\simeq$2.15 rather than $\simeq$2.20). We can conclude that DMAs do not alter the self-similar phase of the collapse (Larson 1969; Penston 1969), at least for run M100 and for $n_c \leq 10^{14}\,cm^{-3}$. The evolution of the DM density profile is in good agreement with previous studies; see for instance fig. 1 in SFG08 and fig. 1 in I08.

It is also relevant to note that (as could be expected) the differences in infall velocity, temperature profile and H_2 fraction affect only the central $\sim 10^4\,M_\odot$ of gas (i.e. the gas within the hexagonal

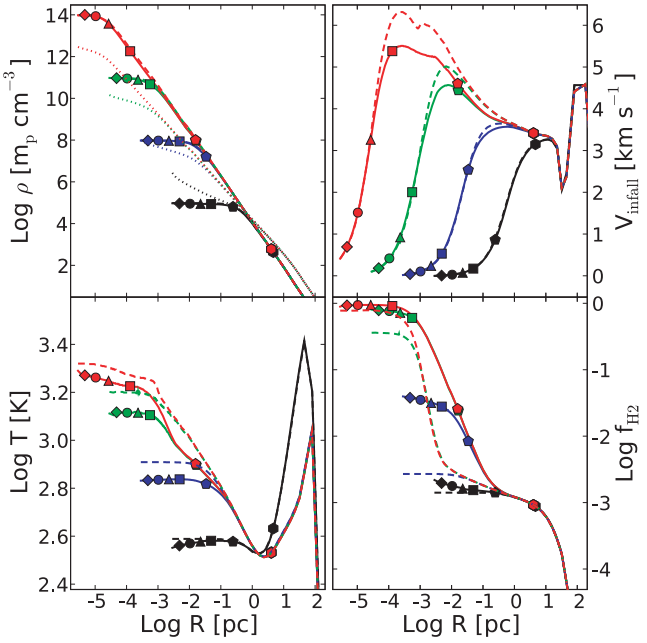

Figure 7. Evolution of DM and gas profile (top left-hand panel), infall velocity (top right-hand panel), temperature (bottom left-hand panel) and H_2 fraction (bottom right-hand panel) during the collapse, comparing runs M100 (fiducial) and NODM (control). Solid lines refer to gas quantities in the M100 case, dashed lines to gas quantities in the NODM control run. Different solid lines refer to central shell gas densities $n_c = 10^5$, 10^8, 10^{11}, 10^{14} cm^{-3}; the different stages can be easily distinguished through the position of their innermost point, as the lines referring to high-density stages extend to lower radii. In the upper left-hand panel, the dotted lines refer to DM densities in the M100 case (note that the DM density profile for the $n_c = 10^5$ cm^{-3} stage is very similar to the NFW profile which is assumed to form immediately after virialization). The geometrical markers indicate the position enclosing baryonic masses of 10^4 M$_\odot$ (hexagons), 10^2 M$_\odot$ (pentagons), 1 M$_\odot$ (squares), 10^{-1} M$_\odot$ (triangles), 10^{-2} M$_\odot$ (circles) and 10^{-3} M$_\odot$ (diamonds); see text for comments.

marks). Actually, relevant (although yet not dramatic) differences are limited to the inner $\sim 10^2$ M$_\odot$ (region within the pentagonal marks): the overall properties of the 10^6 M$_\odot$ halo are conserved in presence of DMAs.

The lower panels visualize the changes in temperature (lower left-hand panel) following the modification of H_2 fraction (lower right-hand panel) which we have extensively commented in the previous sections. Here we only note that the molecular core is significantly more extended than in the control run: the region where H_2 is the dominant chemical species encloses ~ 5 M$_\odot$, rather than ~ 1 M$_\odot$; furthermore, the fall in H_2 abundance is less steep than in the case without DMAs.

The upper right-hand panel is somewhat intriguing, as it gives a glimpse of the modification of the dynamical properties of the collapse: while there are very little changes in the central region (say, within the square marks, corresponding to a 1 M$_\odot$ enclosed mass) and in the outskirts of the halo (at enclosed masses $\gtrsim 10^3$ M$_\odot$, i.e. outside a point roughly mid-way between the pentagonal and hexagonal marks), the infall velocity of the intermediate-mass gas shells is slowed down. The reduced temperature of the cloud (due to the more efficient H_2 cooling which we discussed in the previous sections; see also the bottom right-hand panel of Fig. 7) is likely responsible for this change. In fact, it is well known (see e.g. Stahler, Palla & Salpeter 1986, and references therein) that during the self-similar evolution, the mass infall rate $\rho(r)v_{\rm infall}(r)$ in the region where the density falls as a power law with index ~ 2 should roughly scale with c_s^3/G, where $c_s \propto T^{1/2}$ is the isothermal sound speed. Since $\rho(r)$ is practically the same in the M100 and NODM runs, the reduced temperature should result in a reduced infall velocity, similar to what we obtain.

Table 3. Collapse times (yr) of the innermost gas shell.

log[n_c (cm^{-3})]	NODM	M100	M1
2–3	2.117×10^6	2.116×10^6	2.107×10^6
3–4	8.382×10^5	8.326×10^5	8.077×10^5
4–5	3.204×10^5	3.200×10^5	3.401×10^5
5–6	1.158×10^5	1.177×10^5	1.190×10^5
6–7	3.930×10^4	4.026×10^4	3.895×10^4
7–8	1.261×10^4	1.250×10^4	1.221×10^4
8–9	3.927×10^3	3.757×10^3	3.544×10^3
9–10	1.210×10^3	1.118×10^3	1.072×10^3
10–11	366.4	333.3	333.7
11–12	103.2	102.0	111.3
12–13	29.42	31.93	31.05
13–14	9.210	9.480	–

Note. The time intervals needed for the innermost shell to increment its density of one order of magnitude, in the NODM, fiducial and maximal run. The highest density is absent in the M1 case because the run has been stopped at smaller density, see text.

It is worth noting that on the contrary, the collapse of the innermost gas shell is *accelerated*, albeit very slightly, by the presence of DM, until central densities of 10^{12} cm^{-3} ($/10^{11}$ cm^{-3}) for the M100(/M1) case, see Table 3. However, such infall time alteration are of very small entity, and in any case negligible with respect to the total collapse time – of the order of 3×10^6 yr.

3.4.2 *The maximal run*

Fig. 8, analogue to Fig. 7, compares the control run to the maximal run, rather than to the fiducial run; in this case the highest central density we plot is $n_c = 10^{13}$ cm^{-3} (rather than 10^{14} cm^{-3}) because the maximal run was stopped before reaching $n_c = 10^{14}$ cm^{-3}.

The top left-hand panel shows that even in this case DMAs do not alter the self-similar part of the collapse; however, it should be remarked that the highest density stage is starting to deviate from the expected self-similar profile: in fact, the density profile within the core is not flat, but there is a maximum at the edge of the core.

This is more clear when we examine the other panels: the lines referring to the three stages with $n_c \leq 10^{11}$ cm^{-3} are qualitatively similar to their counterparts in Fig. 7; but the lines representing the highest density stage are clearly different, and we will focus on them.

In the lower panels we can see a huge drop in the H_2 abundance near the centre of the protostar, and a corresponding discontinuity in the gas temperature; both could be expected by our discussion in the previous sections, even if here we get a further piece of information about the size of the region where the H_2 was dissociated ($R \lesssim 3 \times 10^{-5}$ pc, enclosed mass $\sim 3 \times 10^{-2}$ M$_\odot$). Also the velocity panel is affected: this is the only case where the infall velocities of the run with DMAs significantly exceed those in the control run in an extended region; furthermore, we can see that there are secondary peaks in velocity at low radii (in particular one is coincident with the edge of the region where H_2 was dissociated), which are likely to result from the propagation of the density wave which was

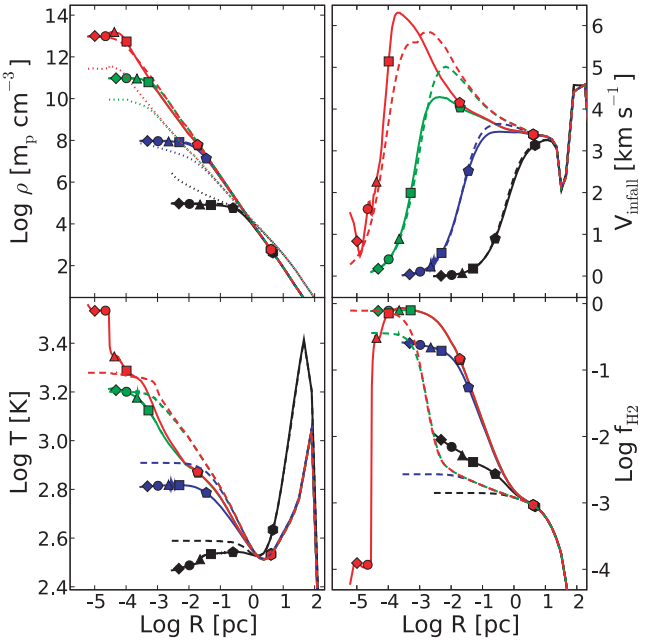

Figure 8. Same as in Fig. 7 but comparing runs M1 (maximal) and NODM (control). Solid lines refer to gas quantities in the M1 run, dashed lines to gas quantities in the NODM control run. All the symbols and lines are the same as in Fig. 7, apart from the fact that the lines extending to the innermost radii refer to a central gas density $n_c = 10^{13}\,\mathrm{cm}^{-3}$ (rather than $10^{14}\,\mathrm{cm}^{-3}$); see text for comments.

generated by the re-expansion of the core which occurred when $n_c \simeq 10^{12}\,\mathrm{cm}^{-3}$.

All these properties indicate that the core of this object is approaching hydrostatical equilibrium, even if it is not quite there. It is interesting to note that the innermost regions of enclosed mass between 1 and $10\,\mathrm{M}_\odot$ are infalling with higher velocity than in the NODM case, whereas between 10 and $10^3\,\mathrm{M}_\odot$ the collapse is slowed, when central density is $n_c = 10^{12}\,\mathrm{cm}^{-3}$. Again, this is equivalent to what we have observed for the fiducial run, and shown in Table 3, and the feature only becomes more pronounced in the case of the maximal run.

4 DISCUSSION

We have studied the effects of self-annihilating DM on the collapse of the gas structures harbouring the formation of the first stars, known as Population III. For the first time in the literature we follow self-consistently the evolution of the DM profile as a consequence of the gravitational drag of the collapsing gas and include the feedback of energy injection by DMAs on the chemistry of the gas, in the yet-unexplored regime between the virialization of the halo and the formation of a hydrostatic core. We have explored the effects of DMAs by spanning a range of masses and annihilation cross-sections around the values of the Vanilla WIMP scenario, namely those able to reproduce the relic abundance of DM with a thermal decoupling, finding similar results but with variations in the details and onset times of the different phases that we are to summarize.

In the following, quoted numbers refer to our fiducial case ($m_{\mathrm{DM}}c^2 = 100\,\mathrm{GeV}$, $\langle\sigma v\rangle = 3 \times 10^{-26}\,\mathrm{cm}^3\,\mathrm{s}^{-1}$, $\kappa = 0.01\,\mathrm{cm}^2\,\mathrm{g}^{-1}$). As expected, heavier WIMPs (or smaller self-annihilation rates, or lower opacity since the energy-injection term is proportional to $\langle\sigma v\rangle/m_{\mathrm{DM}}$ and depends also on κ) effects become relevant at later times during the collapse, the same DMA rate being achieved at higher DM densities. Lighter particles (or higher $\langle\sigma v\rangle$ or higher κ) produce the same effects at earlier times (and therefore smaller gas densities). This general scenario is robust with respect to parameter variations within physically acceptable ranges. A few key points of our study are worth some emphasis: (i) as known from existing literature (RMF07), before the virialization of the halo, at gas density $n_c \lesssim 10^3\,\mathrm{cm}^{-3}$ (and therefore extremely small gas opacity) DMAs do not sensibly affect any gas process; (ii) between halo virialization and a gas density $n_c \sim 10^{11}\,\mathrm{cm}^{-3}$ DMAs contribute mainly through indirect feedback effects: the free-electron floor created by the ionizations induced by DMAs catalyses H_2 formation. In turn, molecular H_2 provides more cooling to the cloud than in the standard case (without DMAs) and the temperature of the cloud *decreases* as a consequence of DMAs; (iii) finally, at $n_c \gtrsim 10^{11}\,\mathrm{cm}^{-3}$ the DMA heating rate becomes equal to the gas cooling rate. To a first approximation this leads to a balance between losses and gain, which we dubbed as the 'critical point'.

Our results generally agree with previous ones: as the semi-analytical estimates of SFG08 and the analytical study (based on simulation data) from Natarajan, Tan & O'Shea (2009), we confirm the existence of a 'critical point'. We also find that the equality of H_2 cooling versus DMA heating terms takes place (in the innermost shell) at central densities of approximately $n_c \sim 10^{12}\,\mathrm{cm}^{-3}$, details depending on parameters (DM mass, opacity coefficient, etc., see previous section and following discussion), in agreement with the above-mentioned studies. This is particularly relevant as our analysis is the first fully numerical, self-consistent study including a reasonably accurate treatment of radiative transfer allowing us to reach the critical point and beyond it in at least three cases.

It had been previously suggested (SFG08) that, after reaching of the 'critical point', the collapse would stop and the whole structure stall, thus generating a new type of celestial object. With our numerical simulations we have accessed this stage of the collapse, finding that the system does *not* halt its collapse in three cases out of four; in the only case where the collapse stops, this happens far after the critical point was reached, and its duration is very short ($\sim$3 yr) after which the gas restarts contracting. Moreover, the DM parameters for which the astrophysical system finds important changes after the critical point are actually strongly disfavoured by DM constraints based on local and primordial Universe observations. By changing the DM mass or self-annihilation rate, the scenario we have described does not change qualitatively, within the range of values studied and the physical regime we have accessed with our simulations.

While stressing again that when our objects reach the critical point the structure does *not* halt the collapse, and instead it continues its evolution towards the formation of a protostellar core, it is also useful to comment on the alteration of the dynamics of the collapse induced by DMAs.

The duration of the gas collapse from halo virialization down to densities of $n_c \sim 10^{14}\,\mathrm{cm}^{-3}$ in presence of DMAs appears to be *shorter* (especially in the first phases) than in the standard case (by about 1 per cent) of the total collapse time. However, we point out that the change is a small fraction of the total, and that the effects of DMAs on collapse time are very difficult to quantify. In fact, the DMAs' effect can indeed accelerate the collapse in some shells, and decelerate it in others, thus making it difficult to obtain a homogeneous definition of time delay. For example, the reduction of the infall velocity of shells enclosing $\sim 10^2\,\mathrm{M}_\odot$ implies that the collapse time of these shells is longer (by 10–20 per cent) than in the control (NODM) case.

We feel confident in stressing, however, that the shells which are mostly affected by the infall time decrease (∼20 per cent of the infall velocity) are placed between 10^2 and $10^3\,M_\odot$, and would become part of a hydrostatic protostar only in the final stages of the collapse. It is not clear whether these shells will eventually end up in the hydrostatic core (Omukai & Palla 2003); however, it is reasonable to expect that such modification will not alter the *total* time for the formation of the star by more than ∼20 per cent.

4.1 Hints about the hydrostatic core

Even if our runs could not reach the regime when a hydrostatic core forms (with the partial exception of the maximal run, where we probably got close), it is worth examining the likely consequences of our results for the further evolution of the protostar in presence of DMAs.

We start reminding that in the standard case (without DMAs) the simulations of R02 show that when the protostar becomes opaque to continuum radiation (at $n_c \simeq 10^{16}\,cm^{-3}$), the formation of the hydrostatic core is delayed by the thermostatic effects of H_2 dissociations, so that the core actually forms when $n_c \gtrsim 10^{20}\,cm^{-3}$.

However, at the end of our runs the central H_2 abundance in the maximal and submaximal runs is ≤ 0.1; even in the fiducial run, the H_2 abundance, while still high, is decreasing much earlier than in the standard case; this is very different from the results of R02, where $f_{H2} \sim 1$ up to $n_c \gtrsim 10^{16}\,cm^{-3}$. Because of the lower amount of H_2, it is reasonable to expect that in the cases with DMAs the delaying effects of H_2 dissociation are absent, or smaller than in the standard case. Then, the hydrostatic core would form at lower densities (e.g. $n_c \sim 10^{16}\,cm^{-3}$, if the protostar becomes optically thick to continuum radiation at the same density as in the R02 runs), and its initial mass would be larger (probably in the 0.01–0.1 $M_\odot$ range, rather than $\simeq 0.003\,M_\odot$).

However, we point out that R02 found that in the case with no DMAs the mass of the hydrostatic core grows very fast, reaching $0.1\,M_\odot$ in less than 3 yr (see e.g. their fig. 6): then, the difference in the initial size is relatively unimportant. It is probably more relevant to note that the lower temperatures and infall velocities of the layers outside the hydrostatic core imply that in the cases with DMAs the accretion rate might be slower than what was found by R02.

5 CONCLUSIONS

We have studied the effects of WIMP DMAs on the evolution of primordial gas clouds hosting the first stars. We have followed the collapse of gas and DM within a $10^6\,M_\odot$ halo virializing at redshift $z = 20$, from $z = 1000$ to slightly before the formation of a hydrostatic core, properly including gas heating/cooling and chemistry processes induced by DMAs, and exploring the dependency of the results on different parameters (DM particle mass, self-annihilation cross-section, gas opacity and feedback strength). Independently of such parameters, when the central baryon density, n_c, is lower than the critical density, $n_{crit} \approx 10^9$–$10^{13}\,cm^{-3}$, corresponding to a model-dependent balance between DMA energy input and gas cooling rate, DMA ionizations catalyse an increase in the H_2 abundance by a factor of ∼100. The increased cooling moderately reduces the temperature (by ≈30 per cent) but does not significantly reduce the fragmentation mass scale. For $n_c \geq n_{crit}$, the DMA energy injection exceeds the cooling, with the excess heat mainly going into H_2 dissociations. In the presence of DMA the transition to the continuum-dominated cooling regime occurs earlier and generally is not associated with abrupt temperature variations. In conclusion, no significant differences are found with respect to the case without DMAs; in particular, and contrary to previous claims, the collapse does not stall and the cloud keeps contracting even when $n_c \gg n_{crit}$. Our simulations stop at central densities $\approx 10^{14}\,cm^{-3}$, and cannot follow the hydrostatic core formation, nor its accretion. At the final simulation stage, the lower temperature/infall velocity of the layers enclosing a mass of $\approx 10^2\,M_\odot$ suggest that DMAs might lead to slightly longer stellar formation time-scales, with a possible ≈20 per cent increase over models without DMAs. The latter finding strengthens our conclusions, although the final answer will come from numerical simulations (hopefully also three dimensional) able to address this very same problem in the yet-unexplored density regime $10^{14} \lesssim n_c \lesssim 10^{18}\,cm^{-3}$.

ACKNOWLEDGMENTS

FI acknowledges support from MIUR through grant PRIN-2006 during the early stages of this work, and from the European Community research programme FP7/2007/2013 within the framework of convention #235878. AB and PM acknowledge financial contribution from contract ASI I/016/07/0. We thank M. Mapelli for stimulating discussions, and the anonymous referee for suggestions which helped the clarity of this paper.

REFERENCES

Abel T., Bryan G. L., Norman M. L., 2002, Sci, 295, 93
Ascasibar Y., 2007, A&A, 462, L65
Bertone G., Hooper D., Silk J., 2005, Phys. Rep., 405, 279
Blumenthal G. R., Faber S. M., Flores R., Primack J. R., 1986, ApJ, 301, 27
Casanellas J., Lopes I., 2009, ApJ, 705, 305
Chen X., Kamionkowski M., 2004, Phys. Rev. D, 70, 043502
Chuzhoy L., 2008, ApJ, 679, L65
Cirelli M., Iocco F., Panci P., 2009, J. Cosmol. Astropart. Phys., 009, 0910
Fairbairn M., Scott P., Edsjo J., 2008, Phys. Rev. D, 77, 047301
Freese K., Spolyar D., Aguirre A., 2008a, J. Cosmol. Astropart. Phys., 0811, 014
Freese K., Bodenheimer P. A., Spolyar D., Gondolo P., 2008b, ApJ, 685, L101
Freese K., Spolyar D., Bodenheimer P. A., Gondolo P., 2009, New J. Phys., 11, 105014
Furlanetto S. R., Johnson Stoever S., 2010, MNRAS, 404, 1869
Furlanetto S. R., Oh S. P., Pierpaoli E., 2006, Phys. Rev. D, 74, 103502
Galli D., Palla F., 1998, A&A, 335, 403
Galli S., Iocco F., Bertone G., Melchiorri A., 2009, Phys. Rev. D, 80, 023505
Glover S. C. O., Jappsen A.-K., 2007, ApJ, 666, 1
Gnedin O. Y., Kravtsov A. V., Klypin A. A., Nagai D., 2004, ApJ, 616, 16
Hollenbach D., McKee C. F., 1979, ApJS, 41, 555
Iocco F., 2008, ApJ, 677, L1
Iocco F., Bressan A., Ripamonti E., Schneider R., Ferrara A., Marigo P., 2008, MNRAS, 390, 1655 (I08)
Larson R. B., 1969, MNRAS, 145, 271
Lattanzi M., Silk J., 2009, Phys. Rev. D, 79, 083523
Lenzuni P., Chernoff D. F., Salpeter E. E., 1991, ApJS, 76, 759
Mapelli M., Ferrara A., 2005, MNRAS, 364, 2
Mapelli M., Ferrara A., Pierpaoli E., 2006, MNRAS, 369, 1719
Marigo P., Aringer B., 2009, A&A, 508, 1539
Myers Z., Nusser A., 2008, MNRAS, 384, 727
Natarajan A., Schwarz D. J., 2008, Phys. Rev. D, 78, 103524
Natarajan A., Tan J. C., O'Shea B. W., 2009, ApJ, 692, 574
Navarro J. F., Frenk C. S., White S. D. M., 1996, ApJ, 462, 563
Omukai K., Nishi R., 1998, ApJ, 508, 141
Omukai K., Palla F., 2003, ApJ, 589, 677
O'Shea B., Norman M. L., 2007, ApJ, 654, 66

Padmanabhan N., Finkbeiner D. P., 2005, Phys. Rev. D, 72, 023508
Palla F., Salpeter E. E., Stahler S. W., 1983, ApJ, 271, 632
Penston M. V., 1969, MNRAS, 144, 425
Ripamonti E., 2007, MNRAS, 376, 709
Ripamonti E., Haardt F., Ferrara A., Colpi M., 2002, MNRAS, 334, 401 (R02)
Ripamonti E., Mapelli M., Ferrara A., 2007a, MNRAS, 374, 1067
Ripamonti E., Mapelli M., Ferrara A., 2007b, MNRAS, 375, 1399 (RMF07)
Ripamonti E., Iocco F., Bressan A., Schneider R., Ferrara A., Marigo P., 2009, Proceedings of Science IDM08, 75 (arXiv:0903.0346)
Scott P., Edsjo J., Fairbairn M., 2009, MNRAS, 394, 82
Shchekinov Y. A., Vasiliev E. O., 2007, MNRAS, 379, 1003
Shull J. M., van Steenberg M. E., 1985, ApJ, 298, 268
Spolyar D., Freese K., Gondolo P., 2008, Phys. Rev. Lett., 100, 051101 (SFG08)
Spolyar D., Bodenheimer P. A., Freese K., Gondolo P., 2009, ApJ, 705, 1031
Stahler S. W., Palla F., Salpeter E. E., 1986, ApJ, 302, 590
Stasielak J., Biermann P. L., Kusenko A., 2007, ApJ, 654, 290
Steigman G., Sarazin C. L., Quintana H., Faulkner J., 1978, AJ, 83, 1050
Taoso M., Bertone G., Meynet G., Ekstrom S., 2008, Phys. Rev. D, 78, 123510
Valdès M., Ferrara A., 2008, MNRAS, 387, L8
Valdès M., Ferrara A., Mapelli M., Ripamonti E., 2007, MNRAS, 377, 245
Yoon S. C., Iocco F., Akiyama S., 2008, ApJ, 688, L1
Yoshida N., Omukai K., Hernquist L., Abel T., 2006, ApJ, 652, 6
Zhang L., Chen X., Lei Y.-A., Si Z.-G., 2006, Phys. Rev. D, 74, 103519

APPENDIX A: APPLICABILITY OF THE ADIABATIC CONTRACTION APPROXIMATION

One of the hypotheses underlying the AC approximation – formally equivalent to the requirement that the angular momentum is conserved, condition that identifies the adiabatic invariant $M(R)R$ (Blumenthal et al. 1986) – is that the orbital time of DM particles should be short with respect to the gravitational potential variation time (which in our case can be identified with the collapse time-scale of the baryons). In the case we are studying, this condition is ensured until baryons reach a central density $n_c \gtrsim 10^5\,\mathrm{cm}^{-3}$ (i.e. until the DM dominates the central potential): after that the two time-scales become of the same order of magnitude, and the above hypothesis is not satisfied.

For densities $n_c \lesssim 10^{10}\,\mathrm{cm}^{-3}$ the adoption of the adiabatic approximation can be justified a posteriori because its results are in reasonable agreement with the ones obtained by 3D simulations (e.g. Abel et al. 2002; O'Shea & Norman 2007, as reported by Natarajan et al. 2009; see later in this appendix). For higher densities, numerical simulations provide no information; but we present a summary of a different approach that can be adopted, and show that even in this case the discrepancy remains tolerable.

The case of a 'fast collapse' (where the baryon collapse time is similar to the free-fall time) was studied by Steigman et al. (1978, see their section IIIb), in the assumptions that (i) the baryons are at rest at $t = 0$ (with negligible velocity dispersion, so that they will collapse in free fall), (ii) the DM contribution to the total mass M is small and (iii) DM particles have a non-negligible velocity dispersion. This case can be treated analytically, and Steigman et al. (1978) obtain that if the radius of the sphere enclosing all the baryons goes from R_i (at time $t = 0$) to R_c (at time $t = t_c$), the ratio of the number $N_{DM,c}$ of DM particles within R_c (at t_c) to the number $N_{DM,i}$ of DM particles within R_i (at $t = 0$) is roughly proportional to $(R_c/R_i)^{3/2}$ (cf. their equations 31 and 32[7]), at least in the limit of $R_c \ll R_i$. Then, the density ρ_{DM} of DM particles should grow asymptotically as $(R_c/R_i)^{-3/2}$, or as $\rho_b^{1/2}$.

We can compare this behaviour to the dependence of the central DM density ($\rho_{DM,c}$) upon the central baryonic density ($\rho_{b,c}$) which can be obtained from the AC formalism: SFG08 find that $\rho_{DM,c} \propto \rho_{b,c}^{0.81}$, and our calculations essentially confirm their result. Then, it is clear that the 'fast-collapse' slope is significantly flatter than what can be inferred from the application of the AC. However, there are some extra facts that need to be kept into account.

(i) For central baryonic number densities $n_c \lesssim 10^5\,\mathrm{cm}^{-3}$ the DM density is larger than the baryonic one, and the application of the AC does not modify the DM density profile.

(ii) The 'fast-collapse' slope was obtained with the assumption of a uniform density profile of both the baryons and the DM, whereas the NFW profile of our initial DM profile is strongly peaked: the calculations of $N_{DM,c}/N_{DM,i}$ by Steigman et al. (1978) likely underestimate the value appropriate in the NFW case; as a consequence, it is likely that the slope of the ρ_{DM}–ρ_b relation is higher than 0.5.

(iii) The DM profile seen in the 3D numerical simulations appears more consistent with the AC predictions than with those of the 'fast-collapse' approach. For example, the innermost DM density shown in fig. 2 of Abel et al. (2002) is a factor of $\sim$10 lower than the baryonic density ($n_b \sim 10^9\,\mathrm{cm}^{-3}$); and the comparison of figs 2 and 4 of Natarajan et al. (2009) gives a somewhat lower difference (a factor of $\sim$5) at a higher baryonic density ($n_b \sim 10^{10}\,\mathrm{cm}^{-3}$). This is consistent with the differences by a factor of $[n_b/(10^5\,\mathrm{cm}^{-3})]^{1-0.81} \sim$ 6–9 predicted by AC, but much smaller than the difference by a factor of $[n_b/(10^5\,\mathrm{cm}^{-3})]^{1-0.5} \sim$ 100–300 predicted using the 'fast-collapse' results.

Then, it appears that the AC approximation can be safely used at least for densities up to $n_c \sim 10^{10}\,\mathrm{cm}^{-3}$. It is quite possible (and even likely) that at higher densities there occurs a transition to the 'fast-collapse' regime. However, the (possible) overestimate of the DM density will be by a factor of $\lesssim [n_c/(10^{10}\,\mathrm{cm}^{-3})]^{0.81-0.5}$. Even in the worst case, this remains reasonable up to the density ($n_c = 10^{14}\,\mathrm{cm}^{-3}$) where we stop our simulations. Furthermore, we remark that the (i) AC approach allows a better comparison with previous studies and (ii) our conclusions on the mild effects of DMAs on the protostellar collapse may only be reinforced by a possible overestimate of DM densities.

[7]Note that the power-law index in equation (32) of Steigman et al. (1978) should be $-3/2$ (and not $-1/2$, as in the paper) since this is the value that can be inferred from the more general equation (31).

This paper has been typeset from a TEX/LATEX file prepared by the author.